Phonon-limited electron mobility in graphene calculated using tight-binding Bloch waves

N. Sule and I. Knezevic

Citation: J. Appl. Phys. **112**, 053702 (2012); doi: 10.1063/1.4747930
View online: http://dx.doi.org/10.1063/1.4747930
View Table of Contents: http://jap.aip.org/resource/1/JAPIAU/v112/i5
Published by the American Institute of Physics.

Phonon-limited electron mobility in graphene calculated using tight-binding Bloch waves

N. Sule[a] and I. Knezevic[b]
Department of Electrical and Computer Engineering, University of Wisconsin-Madison, Madison, Wisconsin 53706, USA

(Received 18 May 2012; accepted 20 July 2012; published online 5 September 2012)

We present a calculation of the electron-phonon scattering rates in ideal monolayer graphene using the third-nearest-neighbor (3NN) tight-binding (TB) electronic Bloch wave functions formed by the analytical carbon $2p_z$ orbitals with an effective nuclear charge of $Z_{\text{eff}} = 4.14$. With these wave functions, the band structure is also represented very accurately over the entire Brillouin zone. By fitting the rates calculated using the TB Bloch wave functions to those calculated by density functional theory (DFT), we extract the "bare" acoustic and optical deformation potential constants, which do not include the effect of the wave function overlap or substrate, to be $D_{\text{ac}} = 12$ eV and $D_{\text{op}} = 5 \times 10^9$ eV/cm, respectively. The phonon-limited electron mobility based on these rates is calculated within the relaxation-time approximation and presented for various doping densities and temperatures, with representative values being of order 10^7 cm^2/Vs (50 K) and 10^6 cm^2/Vs (300 K) at the carrier density of 10^{12} cm^{-2}. The electron mobility values are in good agreement with those reported by DFT and exceed the experimentally obtained values, where the substrate plays an important role. We discuss the utility of the 3NN TB approximation for transport calculations in graphene-based nanostructures. © *2012 American Institute of Physics*. [http://dx.doi.org/10.1063/1.4747930]

I. INTRODUCTION

Graphene has attracted tremendous attention in recent years due to its unique band structure and electronic properties.[1–4] Interest has also been fueled by the prospects of taking advantage of graphene's high carrier mobility[5,6] for device applications.[7,8] In spite of the advances in the understanding of electronic transport in graphene,[9–11] there are still unanswered questions about the nature of the dominant scattering mechanisms that determine the low-field electron mobility[12,13] and the value of the mobility's intrinsic upper limit.[14]

In real graphene samples, mobility is expected to be limited by impurities in the substrate or on the surface of the graphene itself,[4] surface polar phonons,[15,16] or by disorder due to the substrate, such as strain or ripples.[4,13] In the absence of extrinsic factors, the electron mobility in graphene is believed to be limited by scattering from the in-plane acoustic and non-polar optical phonons and the out-of-plane flexural phonons.[17–20] It has been shown that flexural phonons could limit the room temperature mobility at relevant carrier densities to a value of around 10^4 cm^2/Vs.[20] However, the effect of flexural phonons can be effectively suppressed by the presence of strain or tension in the sample, which is a likely explanation of the experimental measurements of mobility in excess of 10^5 cm^2/Vs in suspended samples.[21] The effect of in-plane phonon modes, however, cannot be suppressed; hence, the electron mobility limited by the in-plane acoustic and optical phonons is the intrinsic upper limit of mobility in graphene.

Two approaches have been used to calculate the phonon-limited electron mobility in graphene: (1) Electron-phonon scattering rates were calculated based on Fermi's Golden Rule by assuming electrons to be plane waves[17,18] and (2) the rates were calculated from first principles using density functional theory (DFT).[19] The plane-wave model results in the scattering rates that are simple analytical expressions and depend on various materials parameters. Most of these materials parameters have precisely known values; however, the exact values of the deformation potential constants are not entirely clear.[17] Several reports, in which the acoustic deformation potential constant is determined experimentally based on the temperature slope of the electrical resistivity, put the constant's value in the range of 8–30 eV.[5,21–23] This wide range of values of the acoustic deformation potential constant is likely due to the effect of the surface polar phonons from the substrate.[15,19] Using the acoustic deformation potential in the range of 16–20 eV,[4,17,18,24] the plane-wave model predicts the room-temperature phonon-limited electron mobility to be around 10^5 cm^2/Vs for carrier densities close to 10^{12} cm^{-2}.[17] However, recent experiments have already demonstrated mobilities above those predicted by the plane-wave scattering model.[21,24,25]

In contrast, first-principles calculations predict the intrinsic room-temperature electron mobility in graphene close to 10^6 cm^2/Vs at the same carrier density (10^{12} cm^{-2}).[19] By fitting the analytical form of the scattering rates, based on the assumption that electronic wave functions are plane waves, to the first-principles scattering rates, an effective acoustic deformation potential of 4.5 eV was obtained[19] (the value is close to that obtained from the valence-force model[16]). The effective acoustic deformation potential constant extracted this way

[a]Electronic mail: sule@wisc.edu.
[b]Electronic mail: knezevic@engr.wisc.edu.

in general absorbs an average value of the overlap integral between electronic wave functions.

In this paper, we present a calculation of the electron-phonon scattering rates and the electron mobility in ideal monolayer graphene based on using the tight-binding (TB) Bloch wave functions (BWFs) formed by linear combination of the carbon $2p_z$ wave functions. As the TB approximation is widely used to yield a fairly accurate description of the band structure in graphene,[2,26] it is reasonable to assume that the electronic wave functions are fairly localized near the atomic centers instead of being plane-wave-like. The TB approximation in general provides a significant reduction in computational complexity with respect to DFT and is considered to be a viable atomistic approach[27,28] for band structure calculation in nanostructures with sizes of order tens or hundreds of nanometers, which are generally too large to treat using DFT but where finiteness plays an important role in both band structure and transport. Working with tight-binding Bloch wave functions with well-known analytical forms can be very useful in transport simulations of such nanostructures, where confinement affects the band structure, electronic wave functions, as well as the scattering rates, while the physical parameters, such as the deformation potential constants, remain approximately bulklike.

Here, we form the third-nearest neighbor (3NN) TB BWFs based on the analytical $2p_z$ carbon orbitals with an effective carbon nuclear charge of $Z_{\text{eff}} = 4.14$, obtained by ensuring good agreement between the calculated wave function overlap parameters and those of 3NN TB band structure calculations benchmarked to DFT.[26,29] We then calculate the electron-phonon scattering rates in a manner that transparently separates the "bare" deformation potential constants from the wave function overlap integrals (the latter carry information about anisotropy of the scattering matrix[19]). The acoustic and optical deformation potential constants (D_{ac} and D_{op}, respectively) are varied to obtain the best fit between the calculated tight-binding scattering rates and those calculated based on DFT;[19] the best fit is obtained for $D_{\text{ac}} = 12$ eV and $D_{\text{op}} = 5 \times 10^9$ eV/cm. The phonon-limited electron mobility with the computed TB rates and within the relaxation-time approximation is presented, with representative values of 1.06×10^7 cm^2/Vs (50 K) and 1.54×10^6 cm^2/Vs at (300 K) at the carrier density of 10^{12} cm^{-2}. These values are in good agreement with those reported based on DFT and exceed the experimentally obtained values, in which the substrate effects play an important role.[15]

The paper is organized as follows: In Sec. II, we derive the scattering rates based on the 3NN TB BWFs with the carbon $2p_z$ orbitals and present the details of the numerical computation of the overlap integrals in Sec. II A. The scattering rate calculation and the electron mobility at different carrier densities and temperatures are presented in Sec. III. We conclude with final remarks in Sec. IV.

II. THE TIGHT-BINDING BLOCH WAVE MODEL

The nearest-neighbor $2p_z$-orbital TB description is commonly employed to calculate the band structure of graphene and is fairly accurate for low energies near the K-point.[30,31]

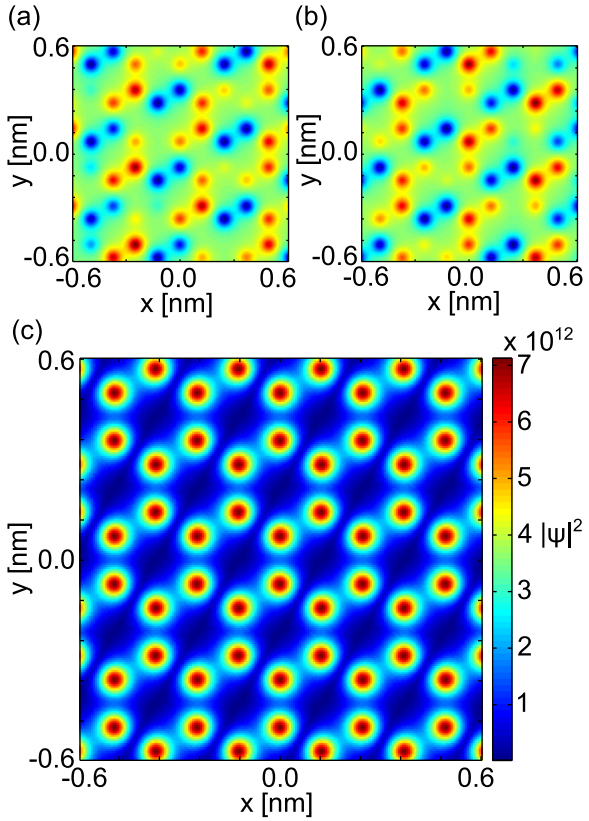

FIG. 1. (a) Real and (b) imaginary parts (red—high, blue—low) of the tight-binding electronic Bloch wave function in graphene as defined in Eq. (1) for $\mathbf{k}$ close to the K-point. (c) Probability density, $|\Psi_{\mathbf{k}}|^2$, associated with the same TB Bloch wave function at a distance of 0.5Å from the carbon atoms plane.

However, the 3NN TB band structure is considerably more accurate over the whole Brillouin zone (BZ).[26,29] The Bloch wave function, $\Psi_{\mathbf{k}}$, used in the TB method is given by

$$\Psi_{\mathbf{k}}(\mathbf{r}) = \sum_{\mathbf{R}} e^{i\mathbf{k}\cdot\mathbf{R}}[e^{i\mathbf{k}\cdot\mathbf{d}_{\text{A}}} b_{\text{A}} \phi(\mathbf{r} - \mathbf{R} - \mathbf{d}_{\text{A}}) + e^{i\mathbf{k}\cdot\mathbf{d}_{\text{B}}} b_{\text{B}} \phi(\mathbf{r} - \mathbf{R} - \mathbf{d}_{\text{B}})], \quad (1)$$

where $\phi(r)$ is the $2p_z$ orbital electronic wave function of carbon, b_{A} and b_{B} are complex coefficients, while $\mathbf{d}_{\text{A}}$ and $\mathbf{d}_{\text{B}}$ are the position vectors of carbon atoms A and B in the unit cell. The Bloch wave function is normalized to unity over the volume of a unit cell. In this work, we calculate the band structure by using the 3NN TB approximation and calculate the overlap parameters based on the $2p_z$ orbital wave function in carbon. The 3NN TB Hamiltonian[32] results in the following secular equations:

$$[E(1 + s_1 g_1) - \gamma_1 g_1 - E_{2p}] b_A + [E(s_0 g_0 + s_2 g_2) - (\gamma_0 g_0 + \gamma_2 s_2)] b_B = 0, \quad (2a)$$

$$[E(s_0 g_0^* + s_2 g_2^*) - (\gamma_0 g_0^* + \gamma_2^* s_2)] b_A + [E(1 + s_1 g_1^*) - \gamma_1 g_1^* - E_{2p}] b_B = 0. \quad (2b)$$

Using the normalization condition and the band structure energies from Eq. (2), we calculate coefficients b_{A} and b_{B} and form the numerical TB BWF. In Figs. 1(a) and 1(b), we

plot the real and imaginary parts of a sample numerical TB BWF with $\mathbf{k}$ near the K-point and in Fig. 1(c) we show the periodic probability density, $|\Psi_{\mathbf{k}}|^2$, of the same TB BWF.

The TB approximation requires knowledge of the overlap parameters, the interaction parameters, and the orbital energy. These parameters are generally either found from experiments or by fitting TB data to first-principles data.[26,29] In Eq. (2), s_0, s_1, and s_2 are the first, second, and third-nearest-neighbor wave function overlap parameters [see Eq. (5) below], γ_0, γ_1, and γ_2 are the corresponding interaction parameters, and E_{2p} is the $2p_z$ orbital energy. The geometric parameters g_0, g_1, and g_2 are defined below, with $\mathbf{a}_1$ and $\mathbf{a}_2$ being the primitive lattice vectors.

$$g_0 = 1 + e^{-i\mathbf{k}\cdot\mathbf{a}_1} + e^{-i\mathbf{k}\cdot\mathbf{a}_2}, \tag{3a}$$

$$g_1 = e^{i\mathbf{k}\cdot\mathbf{a}_1} + e^{i\mathbf{k}\cdot\mathbf{a}_2} + e^{-i\mathbf{k}\cdot\mathbf{a}_1} + e^{-i\mathbf{k}\cdot\mathbf{a}_2} + e^{-i\mathbf{k}\cdot(\mathbf{a}_1+\mathbf{a}_2)}, \tag{3b}$$

$$g_2 = e^{i\mathbf{k}\cdot(\mathbf{a}_1-\mathbf{a}_2)} + e^{i\mathbf{k}\cdot(\mathbf{a}_2-\mathbf{a}_1)} + e^{-i\mathbf{k}\cdot(\mathbf{a}_1+\mathbf{a}_2)}. \tag{3c}$$

We calculate the overlap parameters directly from the $2p_z$ orbital wave-function

$$\phi(r) = \left(\frac{Z_{\text{eff}}}{a_0}\right)^{\frac{5}{2}} \frac{1}{4\sqrt{2}} r\cos\theta e^{-\frac{Z_{\text{eff}} r}{2a_0}}, \tag{4}$$

where a_0 is the Bohr radius and Z_{eff} is the effective nuclear charge of carbon. The optimal value of Z_{eff} is obtained by varying it to find the best agreement between the overlap parameters

$$s_0 = \int d\mathbf{r}\, \phi(\mathbf{r}-\mathbf{d}_A)\phi(\mathbf{r}-\mathbf{d}_B), \tag{5a}$$

$$s_1 = \int d\mathbf{r}\, \phi(\mathbf{r}-\mathbf{d}_A)\phi(\mathbf{r}-\mathbf{d}_A-\mathbf{a}_1), \tag{5b}$$

$$s_2 = \int d\mathbf{r}\, \phi(\mathbf{r}-\mathbf{d}_A)\phi(\mathbf{r}-\mathbf{d}_B-\mathbf{a}_1), \tag{5c}$$

calculated with the $2p_z$ orbitals and those obtained by fitting the first-principles band structure with the 3NN model.[26,29]

Table I shows the values of Z_{eff} and the corresponding values of the overlap parameters calculated using Eq. (5), for which agreement with the 3NN TB data from Refs. 26 and 29 is the best (in Refs. 26 and 29, the 3NN TB band structure was fitted to first-principles calculations). In Ref. 26, the TB parameters are primarily considered to be mathematical fitting parameters, while in Ref. 29 they are considered to be physical entities whose absolute values in the fit must decrease from the second nearest neighbors to the third. Consequently, we get the best agreement with the overlap parameters from Ref. 29, as seen in Table I, for $Z_{\text{eff}} = 4.14$. Fig. 2 shows the band structure calculated using the overlap parameters from Table I and the corresponding interaction parameters taken from Refs. 26 and 29. Although the low-energy, linear dispersion region of the band structure is well-reproduced for all these parameters, the band structure calculated by using $Z_{\text{eff}} = 4.14$ results in the best overall agreement with the corresponding band structure calculated from fitting 3NN TB band structure to first principles data. Having calculated the energies, we then form the numerical TB BWFs. The sample TB BWF shown in Fig. 1 was calculated for $Z_{\text{eff}} = 4.14$ (parameters in row 6 of Table I).

TABLE I. TB overlap parameters calculated using Eq. (5) for different values of Z_{eff} to obtain agreement with the overlap parameters from Refs. 26 and 29, which were found by fitting the 3NN TB band structure to first principles data. Here, "$E < 4$ eV" means that the fitting is accurate for energies below 4 eV and "full BZ" means accuracy over the whole Brillouin zone.

	s_0	s_1	s_2	E_{2p} (eV)
Ref. 26 ($E < 4$ eV)	0.30	0.046	0.039	−2.03
$Z_{\text{eff}} = 2.95$	0.291	0.049	0.024	−1.80
Ref. 26 (full BZ)	0.073	0.018	0.33	−0.28
$Z_{\text{eff}} = 4.67$	0.073	0.0027	0.0007	−0.23
Ref. 29 (full BZ)	0.117	0.004	0.002	−0.45
$Z_{\text{eff}} = 4.14$	0.117	0.007	0.002	−0.45

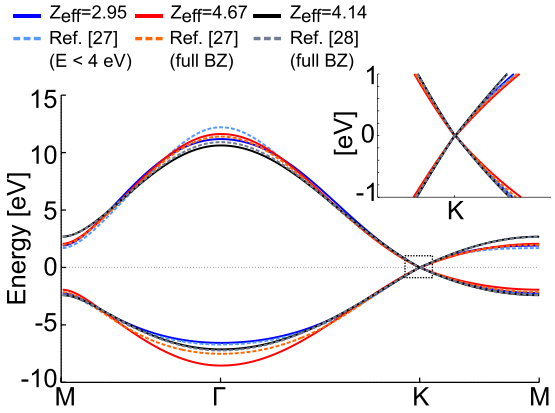

FIG. 2. Band structure of graphene throughout the Brillouin zone. Dashed curves represent the data from Refs. 26 and 29, which have been benchmarked against first-principles calculations. Solid curves correspond to our 3NN tight-binding calculation with the Z_{eff} and the overlap parameters [Eq. (5)] given in Table I. The best overall agreement throughout the Brillouin zone is obtained between the TB calculation with $Z_{\text{eff}} = 4.14$ (black solid curve) and the data from Ref. 29. The inset shows a close-up of the linear band structure region near the K-point; this region is within the dotted rectangle on the main panel.

A. Electron-phonon scattering rates

The Bloch function (1) can be re-written as $\Psi_{\mathbf{q}}(\mathbf{r}) = e^{i(\mathbf{q}+\mathbf{K})\cdot\mathbf{r}} u_{\mathbf{q}}(\mathbf{r})$, where $u_{\mathbf{q}}$ is the periodic part. Here, we have defined $\mathbf{k} = \mathbf{q} + \mathbf{K}$, $\mathbf{K}$ being the wave vector corresponding to the K-point, and $|\mathbf{q}| \ll |\mathbf{k}|$. The change from $\mathbf{k}$ to $\mathbf{q}$ serves to change the origin from the Γ-point to the K-point and having a small $\mathbf{q}$ restricts the calculation to the low-energy, linear dispersion of graphene.

The transition rate between an initial $\Psi_{\mathbf{q}}$ and a final $\Psi_{\mathbf{q}'}$ is given by Fermi's Golden rule:

$$S(\mathbf{q},\mathbf{q}') = \frac{2\pi}{\hbar}|M(\mathbf{q},\mathbf{q}')|^2 \delta[E(\mathbf{q}') - E(\mathbf{q}) \pm \Delta E], \tag{6}$$

where $M(\mathbf{q},\mathbf{q}')$ is the matrix element of the perturbing potential, in our case corresponding to the electron-phonon interaction and given by[33]

$$M(\mathbf{q},\mathbf{q}') = A_\nu(\mathbf{Q})\left[n_\nu(\mathbf{Q}) + \frac{1}{2} \pm \frac{1}{2}\right]^{\frac{1}{2}} I(\mathbf{q},\mathbf{q}'), \tag{7a}$$

$$A_\nu(\mathbf{Q}) = \Delta_\nu(\mathbf{Q})\left[\frac{\hbar}{2A_c\omega_\nu(\mathbf{Q})\rho}\right]^{1/2}, \mathbf{Q} = \mathbf{q}' - \mathbf{q}, \tag{7b}$$

$$I(\mathbf{q},\mathbf{q}') = N_{uc}\int d\mathbf{r}\, u^*_{\mathbf{q}'}(\mathbf{r})u_{\mathbf{q}}(\mathbf{r}). \tag{7c}$$

Here ν represents the phonon branch, $\omega_\nu(\mathbf{Q})$ is the phonon frequency for the phonon wave vector $\mathbf{Q} = \mathbf{q}' - \mathbf{q}$, and $n_\nu(\mathbf{Q})$ is the average occupation of the mode according to the Bose-Einstein distribution. The top sign in Eq. (7a) corresponds to phonon emission, the bottom one to phonon absorption. $A_\nu(\mathbf{Q})$ is a prefactor dependent on the wave vector of the exchanged phonon, $\mathbf{Q}$, A_c is the unit cell area, ρ is the mass density of graphene, and N_{uc} in Eq. (7c) is the number of unit cells. In Eq. (7b)

$$\Delta_{ac} = \pm iD_{ac}|\mathbf{Q}|, \quad \Delta_{op} = D_{op}, \tag{8}$$

where D_{ac} and D_{op} are the "bare" acoustic and optical deformation potential constants, respectively, where by "bare" we mean that they are the constants that appear in the electron-phonon interaction Hamiltonians for longitudinal acoustic and optical phonons $\hat{H}_{e\text{-}ac} = D_{ac}\nabla\hat{\mathbf{u}}$, $\hat{H}_{e\text{-}op} = D_{op}\hat{u}_{||}$, with $\hat{\mathbf{u}}$ ($\hat{u}_{||}$) being the ion displacement operator (its component parallel to the wave propagation direction).[33] Note that we have separated the localized wave function overlap $I(\mathbf{q},\mathbf{q}')$ [Eq. (7c)] from the deformation potential; the overlap integral gives rise to the anisotropy of the matrix elements that was depicted, for instance, in Fig. 1 of Ref. 19. It is also important to note that when the deformation potential constants are extracted experimentally from, for instance, the temperature slope of the resistivity, these are not the "bare" deformation potential values, but rather values that already contain an effective, averaged overlap integral.[19]

The overlap integral [Eq. (7c)] between TB BWFs is calculated by numerical integration over a unit cell, as the TB BWFs are normalized over that volume (more detail in Sec. II B). The scattering rate is found by integrating the transition rate, $S(\mathbf{q},\mathbf{q}')$ [Eq. (6)], over the magnitude and the angle θ' of the outgoing wave vector $\mathbf{q}'$.[34] The energy-conserving delta-function can be simplified by using the linear electronic dispersion of graphene near the K-point. We assume acoustic phonon scattering to be elastic and the phonons to have a linear dispersion.[34] In the elastic and equipartition approximation, we get the following expression for the total scattering rate by acoustic phonons:

$$\tau^{-1}_{ac}(\mathbf{q}) = \frac{D^2_{ac}k_BT|\mathbf{q}|}{2\pi\rho v_s^2\hbar^2 v_F}\int d\theta'\,|I(\mathbf{q},\mathbf{q}')|^2, \quad |\mathbf{q}'| = |\mathbf{q}|. \tag{9}$$

Here, v_s is the sound velocity and v_F is the Fermi velocity in graphene. It should be noted that the equipartition approximation ($\hbar\omega_\mathbf{Q} \ll k_BT$, so $n(\mathbf{Q}) \approx k_BT/\hbar\omega_\mathbf{Q}$) is justified at temperatures significantly above the Bloch-Grüneisen temperature, T_{BG}. For graphene, $T_{BG} \approx 54\,\mathrm{K}\sqrt{n}$, with n being the carrier density in the units of $10^{12}\,\mathrm{cm}^{-2}$ (see, for instance, Refs. 17 and 23). The equipartition approximation is therefore accurate near room temperature over a wide range of carrier densities (see Fig. 4), but at low temperatures and high carrier densities this approximation should be considered qualitative.

Assuming dispersionless optical phonons, we get the following expression for the electron-optical phonon scattering rate (as before, top sign denotes emission, bottom absorption):

$$\tau^{-1}_{op}(\mathbf{q}) = \frac{D^2_{op}}{4\pi\hbar v_F\rho\omega_0}\left(n_0 + \frac{1}{2} \pm \frac{1}{2}\right)\left(|\mathbf{q}| \mp \frac{\omega_0}{v_F}\right) \times \int d\theta'\,|I(\mathbf{q},\mathbf{q}')|^2, \quad |\mathbf{q}'| = |\mathbf{q}| \mp \frac{\omega_0}{v_F}. \tag{10}$$

The derivation of the scattering rate above follows the common procedure employed for nonpolar semiconductors. However, optical phonons in graphene are strongly screened and exhibit the Kohn anomaly and a violation of the Born-Oppenheimer approximation.[35,36] We can account for the effect of screened electron-phonon interaction to an extent through the deformation potential constant: we extract the deformation potential constant by fitting Eq. (10) to the scattering rate computed from DFT,[19] as the DFT rate partly accounts for the screening.

Similarly, for dispersionless, zone-boundary phonons that are responsible for high-momentum transfer intervalley scattering, we get the following rate for scattering between the two equivalent valleys at the K and K' points:

$$\tau^{-1}_{iv}(\mathbf{q}) = \frac{D^2_{iv}}{4\pi\hbar v_F\rho\omega_{iv}}\left(n_{iv} + \frac{1}{2} \pm \frac{1}{2}\right)\left(|\mathbf{q}| \mp \frac{\omega_{iv}}{v_F}\right) \times \int d\theta'\,|I(\mathbf{q},\mathbf{q}')|^2, \; |\mathbf{q}' + \mathbf{K}'| = |\mathbf{q} + \mathbf{K}| \mp \frac{\omega_{iv}}{v_F}. \tag{11}$$

ω_0 and ω_{iv} are the dispersionless optical phonon and intervalley phonon frequency, respectively, while n_0 and n_{iv} are the corresponding phonon occupation numbers at a given temperature. For the intervalley scattering rate in Eq. (6), $\mathbf{q}$ is picked from the valley at K-point, whereas $\mathbf{q}'$ is picked from the valley at K'-point. The intervalley scattering rate at room temperature is negligible with respect to the scattering rates with acoustic and optical phonons because the calculated overlap integral when $\mathbf{q}$ and $\mathbf{q}'$ belong to different valleys is extremely small,[4] so we will ignore intervalley scattering in the rest of the paper.

B. Numerical implementation

We begin by initializing the graphene lattice in real space with primitive lattice vectors $\mathbf{a}_1 = \frac{3a}{2}\hat{x} + \frac{\sqrt{3}a}{2}\hat{y}$ and $\mathbf{a}_2 = \frac{3a}{2}\hat{x} - \frac{\sqrt{3}a}{2}\hat{y}$. We use close to 40 000 unit cells in the real-space lattice and, consequently, the same number of $\mathbf{k}$'s in the first BZ. Of those, about 1000 $\mathbf{k}$'s are used to calculate

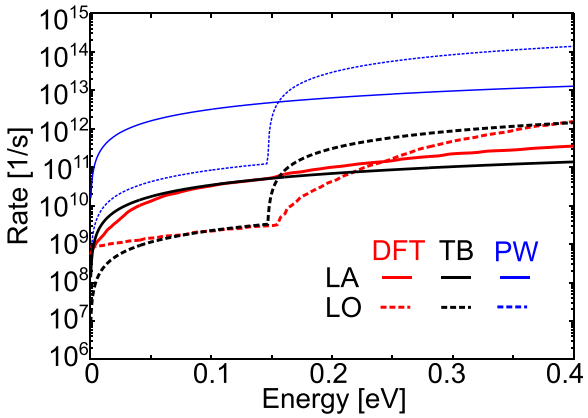

FIG. 3. Scattering rates of electrons with longitudinal acoustic (LA, solid curves) and longitudinal optical (LO, dashed curves) phonons in graphene. For the "bare" deformation potential constants $D_{ac} = 12\,\text{eV}$ and $D_{op} = 5 \times 10^9$ eV/cm, the rates calculated based on the tight-binding Bloch wave model (TB, black curves) follow closely those obtained from the density functional theory in Ref. 19 (DFT, red curves). The TB rates are lower than the plane-wave scattering rates calculated with the same deformation potentials (PW, blue curves) by two orders of magnitude, which indicates that the values of the angle-averaged overlap integrals $\int d\theta' |I(\mathbf{q}, \mathbf{q}')|^2$ in Eqs. (9) and (10) are of order 10^{-2}.

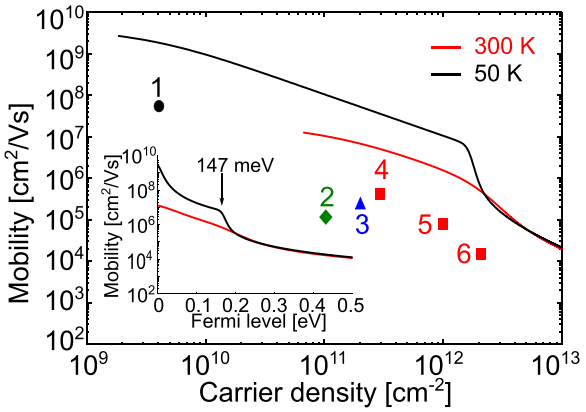

FIG. 4. Electron mobility at 300 K (red) and 50 K (black) as a function of the carrier density, calculated within the relaxation-time approximation with the scattering rates computed using the TB Bloch wave functions. The deformation potential constants used are $D_{ac} = 12\,\text{eV}$ and $D_{op} = 5 \times 10^9 \text{eV/cm}$ (same as in Fig. 3); their values have been found by fitting the TB rates to the DFT model (see Fig. 3). The data points correspond to experimental mobility values reported in the following references: 1—Ref. 14 (temperature 50 K), 2—Ref. 21 (temperature 240 K), 3—Ref. 6 (temperature 5 K), 4—Ref. 25, 5—Ref. 24, 6—Ref. 37 (data points 4, 5, and 6 are all at 300 K). (inset) Electron mobility versus the Fermi level at 50 K and 300 K, revealing that the kink in the low-temperature mobility on the main graph stems from the onset of the optical phonon emission (optical phonon energy taken to be 147 meV).

the energies restricted to below 1 eV (the linear electronic dispersion region of graphene). Next, we determine the b_A and b_B coefficients of the TB BWF from Eq. (2) and the normalizing condition.

The overlap integral, $I(\mathbf{q}', \mathbf{q})$, in Eq. (7c) for a given $\mathbf{q}$ and $\mathbf{q}'$ consists of four terms. Each of these terms consists of sums over all pairs of lattice vectors times an integration involving atomic wave functions corresponding to each of those pairs. The integration is a function of the difference between a given pair of lattice vectors only; therefore, to speed up the calculation, we pre-calculate this integral for a given $\mathbf{q}$ and $\mathbf{q}'$, with one lattice vector fixed at zero and the other going over only those neighbors for which the overlap of the $2p_z$ wave functions is greater than 10^{-13}.

The numerical integration is done by using the trapezoidal method in 3D over a volume that is the area of a unit cell times 2 Å both above and below the lattice. The peak of the probability density of the $2p_z$ orbital in carbon is about 0.7 Å away from the graphene sheet on both sides; therefore, the z-direction thickness of 4 Å essentially includes the complete $2p_z$ orbitals. We calculate the overlap integral only for those pairs of $\mathbf{q}$ and $\mathbf{q}'$ that satisfy the energy conservation for a given scattering process. The integration over angle θ' in Eqs. (9), (10), and (6) is carried out numerically by summing over those values of $I(\mathbf{q}, \mathbf{q}')$ that remain after the energy conservation is satisfied and all have the same magnitude of $\mathbf{q}'$. In order to obtain the scattering rate as a function of energy, we average over all $\mathbf{q}$ that have the same magnitude (i.e., lie on the isoenergy circle).

III. SCATTERING RATES AND THE ELECTRON MOBILITY

In order to extract the "bare" deformation potential constants for graphene that do not implicitly contain any information about the substrate or the overlap of the electronic wave functions, we fit the TB model scattering rates to those calculated using DFT in Ref. 19. Fig. 3 shows the plots of the TB Bloch-wave model scattering rates fitted to the rates calculated using DFT. We extract the following values for the deformation potential constants: $D_{ac} = 12\,\text{eV}$ and $D_{op} = 5 \times 10^9 \text{eV/cm}$. The fitting is approximate as the TB rates assume linear electron dispersion, as well as linear-dispersion acoustic and dispersionless optical phonons, in contrast to the DFT calculation that employs the full electron and phonon dispersions[19] [it should also not be forgotten that DFT has limitations in the excited (conduction band) states calculations]. Overall, the deformation potential constants we extract by fitting to DFT are approximate.

Figure 3 also shows a comparison between the total electron-phonon scattering rates calculated by using the TB model and the plane-wave model [overlap integral in Eq. (7c) equal to 1] with the same deformation potential constants. The plane-wave rates are about two orders of magnitude greater than the TB rates for both LA and for LO scattering, meaning that the angle-averaged overlap integrals $\int d\theta' |I(\mathbf{q}, \mathbf{q}')|^2$ in Eqs. (9) and (10) are of order 10^{-2}. Other parameters used for all curves in Fig. 3 are temperature $T = 300\,\text{K}$, mass density $\rho = 7.6 \times 10^7\,\text{g/cm}^2$, sound velocity for longitudinal acoustic phonons $v_s = 2 \times 10^6\,\text{cm/s}$, Fermi velocity $v_F = 10^8\,\text{cm/s}$, optical phonon energy $\hbar\omega_0 = 147$ meV [extracted from Fig. 2(a) of Ref. 19 as the threshold energy for LO phonon emission].

Finally, we calculate the low-field electron mobility in graphene as a function of the carrier density based on the relaxation-time approximation (RTA)[34]

$$\mu = \frac{ev_F^2}{2k_BT} \frac{\int dE \frac{\tau(E)\exp\left(\frac{E-E_F}{k_BT}\right)}{\left[1+\exp\left(\frac{E-E_F}{k_BT}\right)\right]^2}}{\int dE \frac{E}{\left[1+\exp\left(\frac{E-E_F}{k_BT}\right)\right]^2}}, \quad (12)$$

where $\tau^{-1}(E) = \tau_{ac}^{-1}(E) + \tau_{op}^{-1}(E)$ is the total scattering rate, which we calculate using the TB Bloch waves [Eqs. (9) and (10)]. The results are shown in Fig. 4 for 300 K and 50 K. The data points on the plot represent several experimentally obtained values of the electron mobility.[6,14,21,24,25,37] Transport measurements on graphene are affected by charge inhomogeneties from spurious chemical doping or invasive metal contacts, and measurement errors are especially pronounced near the charge-neutrality point.[38]

The kink in the low-temperature mobility stems from the onset of the optical phonon emission, as shown in the inset, which depicts the mobility vs. Fermi level dependence. As the rates were closely matched to the DFT rates, the obtained mobilities are also very similar in value to the DTF ones and higher than experimental values, which include the effects of the substrate. It is also worth noting that we have included only LA and LO phonons in this calculation. However, the DFT data indicate that the TA and TO scattering rates are actually comparable to their longitudinal counterparts, so, with their inclusion, a roughly twofold drop in the calculated mobility could be expected.

IV. CONCLUSION

In summary, we have presented a simple model for calculating the electron-phonon scattering rates and electron mobility in graphene based on using electronic 3NN TB BWFs. By fitting the TB rates to those calculated from first-principles,[19] we were able to extract the values of the "bare" deformation potential constants, which will be important for the calculation of electron-phonon scattering rates in nanostructured graphene, where the electronic wave functions are confined while many physical constants can be assumed bulklike.

It should be remembered that 3NN TB analytical $2p_z$ orbitals are almost certainly an over-simplification of graphene wave functions, even though the bulk band structure based on them is accurate. TB calculations do not capture fully the nature of carbon resonant bonds, as evidenced, for example, by incorrect TB predictions of the band gap's chirality dependence in armchair nanoribbons.[39,40] With this caveat in mind (or, ideally, with an improved way to treat the complex physics of graphene edge states[40]), the 3NN TB model could still be useful in calculating the band structure and electronic wave functions in systems such as graphene nanoribbons, which are not suitable for DFT calculations because of their large size (width can be tens to hundreds of nanometers, length even micron-size[41]) and line edge roughness[42] that precludes treatment of the ribbon as periodic. Moreover, as the 3NN TB model with analytical $2p_z$ orbitals enables easy construction of wave functions, it can provide a less computationally intensive alternative to first-principles approaches when it comes to calculating the scattering rates for semiclassical[43] or quantum[44] transport simulation in realistic devices, where a very fine sampling of the Brillouin zone for both initial and final states is needed.

ACKNOWLEDGMENTS

The authors thank Z. Aksamija for valuable discussions. This work has been supported by the NSF through the University of Wisconsin MRSEC (Grant No. DMR-0520527) and by the AFOSR [Grant Nos. FA9550-09-1-0230 (YIP program) and FA9550-11-1-0299].

[1] K. S. Novoselov and A. K. Geim, Nat. Mater. **6**, 183 (2007).
[2] A. H. C. Neto, F. Guinea, N. M. R. Peres, K. S. Novoselov, and A. K. Geim, Rev. Mod. Phys. **81**, 109 (2009).
[3] M. J. Allen, V. C. Tung, and R. B. Kaner, Chem. Rev. **110**, 132 (2010).
[4] S. D. Sarma, S. Adam, E. H. Hwang, and E. Rossi, Rev. Mod. Phys. **83**, 407 (2011).
[5] X. Hong, A. Posadas, K. Zou, C. H. Ahn, and J. Zhu, Phys. Rev. Lett. **102**, 136808 (2009).
[6] K. I. Bolotin, K. J. Sikes, Z. Jiang, M. Klima, G. Fudenberg, J. Hone, P. Kim, and H. L. Stormer, Solid State Commun. **146**, 351 (2008).
[7] A. K. Geim, Science **324**, 1530 (2009).
[8] X. Li, X. Wang, L. Zhang, S. Lee, and H. Dai, Science **319**, 1229 (2008).
[9] S. Adam, E. H. Hwang, V. M. Galitski, and S. D. Sarma, Proc. Natl. Acad. Sci. **104**, 18392 (2007).
[10] S. Adam and S. D. Sarma, Phys. Rev. B **77**, 115436 (2008).
[11] D. A. Areshkin, D. Gunlycke, and C. T. White, Nano Lett. **7**, 204 (2007).
[12] Z. H. Ni, L. A. Ponomarenko, R. R. Nair, R. Yang, S. Anissimova, I. V. Grigorieva, F. Schedin, P. Blake, Z. X. Shen, E. H. Hill, K. S. Novoselov, and A. K. Geim, Nano Lett. **10**, 3868 (2010).
[13] E. R. Mucciolo and C. H. Lewenkopf, J. Phys.: Condens. Matter **22**, 273201 (2010).
[14] P. Neugebauer, M. Orlita, C. Faugeras, A.-L. Barra, and M. Potemski, Phys. Rev. Lett. **103**, 136403 (2009).
[15] X. Li, E. A. Barry, J. M. Zavada, M. B. Nardelli, and K. W. Kim, Appl. Phys. Lett. **97**, 232105 (2010).
[16] V. Perebeinos and P. Avouris, Phys. Rev. B **81**, 195442 (2010).
[17] E. H. Hwang and S. D. Sarma, Phys. Rev. B **77**, 115449 (2008).
[18] R. S. Shishir and D. K. Ferry, J. Phys.: Condens. Matter **21**, 232204 (2009).
[19] K. M. Borysenko, J. T. Mullen, E. A. Barry, S. Paul, Y. G. Semenov, J. M. Zavada, M. B. Nardelli, and K. W. Kim, Phys. Rev. B **81**, 121412 (2010).
[20] E. V. Castro, H. Ochoa, M. I. Katsnelson, R. V. Gorbachev, D. C. Elias, K. S. Novoselov, A. K. Geim, and F. Guinea, Phys. Rev. Lett. **105**, 266601 (2010).
[21] K. I. Bolotin, K. J. Sikes, J. Hone, H. L. Stormer, and P. Kim, Phys. Rev. Lett. **101**, 096802 (2008).
[22] J.-H. Chen, C. Jang, S. Xiao, M. Ishigami, and M. S. Fuhrer, Nat. Nanotechnol. **3**, 206 (2008).
[23] D. K. Efetov and P. Kim, Phys. Rev. Lett. **105**, 256805 (2010).
[24] F. Chen, J. Xia, D. K. Ferry, and N. Tao, Nano Lett. **9**, 2571 (2009).
[25] S. V. Morozov, K. S. Novoselov, M. I. Katsnelson, F. Schedin, D. C. Elias, J. A. Jaszczak, and A. K. Geim, Phys. Rev. Lett. **100**, 016602 (2008).
[26] S. Reich, J. Maultzsch, C. Thomsen, and P. Ordejón, Phys. Rev. B **66**, 035412 (2002).
[27] T. Boykin, G. Klimeck, and F. Oyafuso, Phys. Rev. B. **69**, 115201 (2004).
[28] T. B. Boykin, M. Luisier, G. Klimeck, X. Jiang, N. Kharche, Y. Zhou, and S. K. Nayak, J. Appl. Phys. **109**, 104304 (2011).
[29] R. Kundu, Mod. Phys. Lett. B **25**, 163 (2011).
[30] P. R. Wallace, Phys. Rev. **71**, 622 (1947).
[31] H. Zheng, Z. F. Wang, T. Luo, Q. W. Shi, and J. Chen, Phys. Rev. B **75**, 165414 (2007).
[32] R. Saito, G. Dresselhaus, and M. Dresselhaus, *Physical Properties of Carbon Nanotubes* (Imperial College, 1998).
[33] B. R. Nag, *Electron Transport in Compound Semiconductors* (Springer, 1980).
[34] M. Lundstrom, *Fundamentals of Carrier Transport* (Cambridge University, 2000).
[35] S. Pisana, M. Lazzeri, C. Casiraghi, K. S. Novoselov, A. K. Geim, A. C. Ferrari, and F. Mauri, Nat. Mater. **6**, 198 (2007).
[36] A. C. Ferrari, Solid State Commun. **143**, 47 (2007).

[37]K. S. Novoselov, A. K. Geim, S. V. Morozov, D. Jiang, Y. Zhang, S. V. Dubonos, I. V. Grigorieva, and A. A. Firsov, Science **306**, 666 (2004).
[38]P. Blake, R. Yang, S. V. Morozov, F. Schedin, L. A. Ponomarenko, A. A. Zhukov, R. R. Nair, I. V. grigorieva, K. S. Novoselov, and A. K. Geim, Solid State Commun. **149**, 1068 (2009).
[39]V. Barone, O. Hod, and G. E. Scuseria, Nano. Lett. **6**, 2748 (2006).
[40]Y.-W. Son, M. L. Cohen, and S. G. Louie, Phys. Rev. Lett. **97**, 216803 (2006).
[41]M. Y. Han, B. Özyilmaz, Y. Zhang, and P. Kim, Phys. Rev. Lett. **98**, 206805 (2007).
[42]X. Wang, Y. Ouyang, X. Li, H. Wang, J. Guo, and H. Dai, Phys. Rev. Lett. **100**, 206803 (2008).
[43]C. Jacoboni and L. Reggiani, Rev. Mod. Phys. **55**, 645 (1983).
[44]H. Haug and A. Jauho, *Quantum Kinetics in Transport and Optics of Semiconductors*, Springer Series in Solid-State Sciences Vol. 6 (Springer, 2008).